Progress In Electromagnetics Research C, Vol. 111, 241–256, 2021

Wideband Dual Polarized Compact Design of Pi-Shape Microstrip Antenna for GSM, ISM, and Satellite Applications

Aarti G. Ambekar* **and Amit A. Deshmukh**

Abstract—The design of a compact Pi-shape microstrip antenna for dual-polarized wideband response is proposed. The Pi-shape geometry is realized by modifying a compact C-shape patch. The two stubs placed on the Pi-shape patch edge optimize the spacing in between the higher order TM_{20} and TM_{30} resonant modes with respect to the fundamental TM_{10} mode which yield a bandwidth of more than 430 MHz ($> 35\%$). On an air suspended substrate, the antenna exhibits broadside gain of more than 5 dBi over the impedance bandwidth. The orthogonal surface current variations across the TM_{10}, TM_{20}, and TM_{30} modes realize polarization agility satisfying the requirements of GSM900/navigation satellite applications/ISM900. With respect to the band start frequency, the proposed configuration offers 11% reduction as compared with the equivalent rectangular microstrip antenna. Further, by defining the resonant length at each of the Pi-shape patch modes, the formulation for their resonant frequency is proposed. The Pi-shape antennas redesigned using them at the given fundamental mode frequency yield similar dual polarized wideband responses offering bandwidth of $> 35\%$.

1. INTRODUCTION

The growing demand for the wireless communication systems and applications requires more efficient and smaller antenna designs. Many wireless applications need compact radiating structures offering polarization agility along with a wider impedance bandwidth (BW). Microstrip antenna (MSA) is one of the best candidates for these requirements because of its low-profile nature and ease of integration with microwave integrated circuits [1–4]. Several techniques like the use of stack resonators [5, 6], slot or stub loaded MSAs [7–11], and different probe feeding techniques [12] have been reported for the realization of wider BW, offering polarization agility. The use of parasitic metallic cone and two microstrip feed lines [13], or the combination of multiple patch parameters along with a modified feeding technique [14–17], leads to a complex design for realizing the dual-polarized (DP) wideband response. A compact and wideband design of DP MSA by using overlapped parasitic patches is reported [18]. Here the reported work does not explain the effects of overlapped patch dimensions on the modified patch resonant modes, in realizing this wider BW. Although being fabricated on a thicker substrate, the BW realized in the design reported in [19] is smaller. A wideband DP MSA employing shorting pins and embedded slots as reported in [20–22] does not provide an in depth explanation about the antenna working in terms of the shorted patch modes. Wider BW reconfigurable MSAs as reported in [23, 24] are complex due to the biasing circuits present.

In this paper, initially a proximity fed configuration of basic Pi-shape MSA is discussed on an air suspended FR4 substrate of total thickness $0.1\lambda_g$. An N-type connector is used for feeding the patch. The resonant modes of the basic Pi-shape MSA are analyzed. At the fundamental mode, a BW of 215 MHz (18%) is obtained. To explore the possibility of dual-polarized wideband response, stubs are loaded on the edges of the Pi-shape MSA. The stub positions are appropriately selected such that they

Received 23 February 2021, Accepted 2 April 2021, Scheduled 11 April 2021
* Corresponding author: Aarti G. Ambekar (arti1910@gmail.com).
The authors are with the EXTC Department, SVKM's DJSCE, Mumbai, India.

tune the higher order TM_{20} and TM_{30} mode frequencies with respect to the fundamental TM_{10} mode, to realize wider BW. The optimized single stub design covers a frequency span of 885 to 1220 MHz yielding impedance BW of 335 MHz (30%) while the two-stub configuration covers a frequency span of 874 and 1315 MHz yielding BW of 441 MHz (40%). Both the configurations exhibit a broadside radiation pattern over the BW with a gain of more than 6 dBi. The proposed configuration yields polarization diversity as the E plane is directed along $\Phi = 0°$ at TM_{10} mode while along 90° at TM_{20} and TM_{30} modes. By studying the surface current distribution at various modes, their resonant length formulation is derived which is followed by the redesigning guidelines for similar dual-polarized wideband Pi-shape MSAs. The antennas designed using the proposed methodology show similar dual-polarized wideband responses. The proposed compact MSA could be promising for a number of wireless application bands like GSM900 (890–960 MHz), navigation satellite bands (1164–1215 MHz and 1215–1240 MHz), and ISM 900 MHz band (902–928 MHz). Thus, the originality of the present work lies in providing an in depth explanation for the realization of the dual-polarized wideband response by analyzing the higher order modes of the compact Pi-shape MSA. The tuning of the respective BW and polarization is achieved by varying the stub lengths. With respect to the band start frequency, the proposed design offers 11% reduction in the frequency as compared to the equivalent rectangular microstrip antenna (RMSA). A simple modification in the patch geometry makes the proposed design simpler in implementation than the reported dual-polarized wideband MSAs. A detailed comparison highlighting the novelty is presented further in the paper. The proposed configuration is first studied using CST Microwave Studio [25]. In the simulation and measurement, a square ground plane of side length 30 cm is used. The high frequency instruments, namely ZVH-8, FSC 6, and SMB-100A, are used in the experimental verification. Radiation pattern and gain measurements are carried out using reference horn antennas. Three antenna method is used in the gain measurement. For various results, a good agreement is obtained between the simulation and measurements.

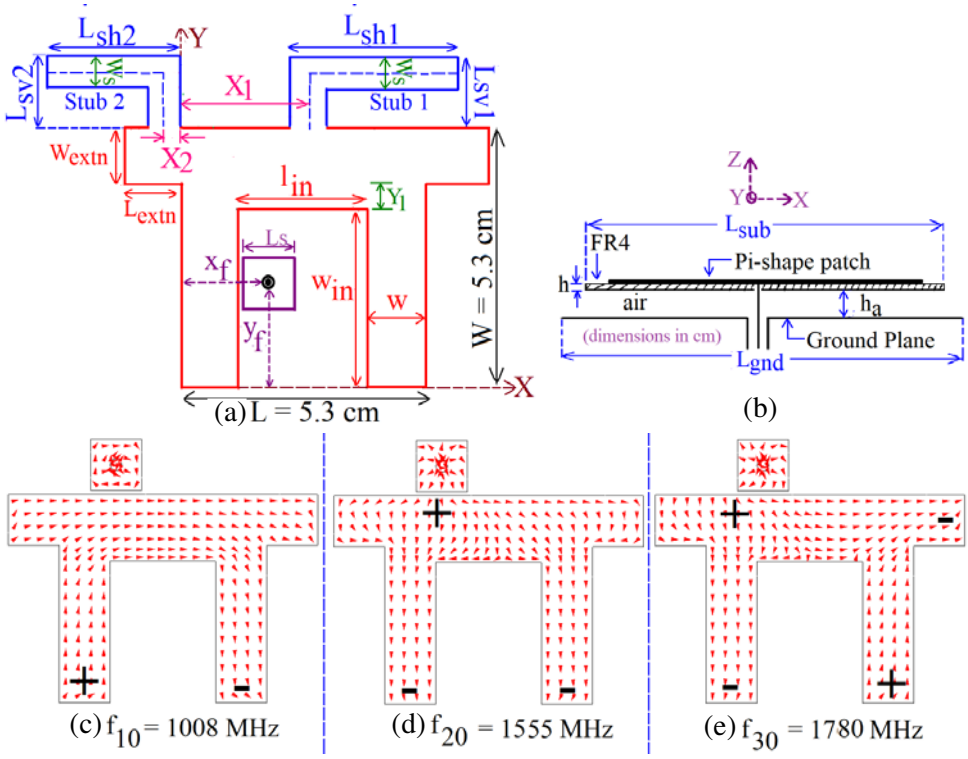

Figure 1. (a) Top and (b) side views of Pi-shape MSA and its (c)–(e) surface current distributions at observed resonant modes.

2. DUAL POLARIZED WIDEBAND PI-SHAPE MICROSTRIP ANTENNA

The proximity fed configuration of a Pi-shape MSA is shown in Figs. 1(a) and (b). The units for the patch dimensions and frequencies referred to in this paper are in 'cm' and 'MHz', respectively. The proposed structure is fabricated on an FR4 substrate (ε_r = 4.3, h = 0.16 cm), which is suspended above the ground plane using an air gap (h_a) of 3.1 cm. The C-shape MSA is a compact variation of rectangular MSA [2]. By suitably modifying the C-shape MSA, a Pi-shape MSA is realized. For the fundamental TM_{10} mode frequency of around 1000 MHz, dimensions of the Pi-shape MSA are parametrically optimized as 'L' = 'W' = 5.3, 'w' = 1.3, 'l_{in}' = 2.7, 'w_{in}' = 3.6, 'Y_1' = 0.4, 'L_{extn}' = 'W_{extn}' = 1.3, 'L_{sub}' = 17.0, and 'W_{sub}' = 7.5 cm. For reducing the fabrication complexity, the proximity strip is placed in the same layer as that of the patch, as shown in Fig. 1(a). Initially, a square strip of dimensions 'L_s' = 1.3 cm is selected.

To begin with, the Pi-shape MSA is simulated for 'x_f, y_f' = 1.7, 7.0 cm, and the surface current distributions at the three observed resonant modes are shown in Figs. 1(c)–(e). The '+' and '−' signs in the current plots indicate the field polarity. The distribution shows integer multiples of half-wavelength variations in the surface currents. The modes are referred to as TM_{n0}, where n = 1, 2, and 3. The modal indices 'n' indicate the integer number of half-wavelength variations along the total Pi-shape length. The patch width is much smaller than its orthogonal dimension, and hence the frequencies corresponding to those modes exhibiting multiples of half-wavelength variations will be observed at much higher frequencies. Hence, those modal variations are not considered for the given frequency range.

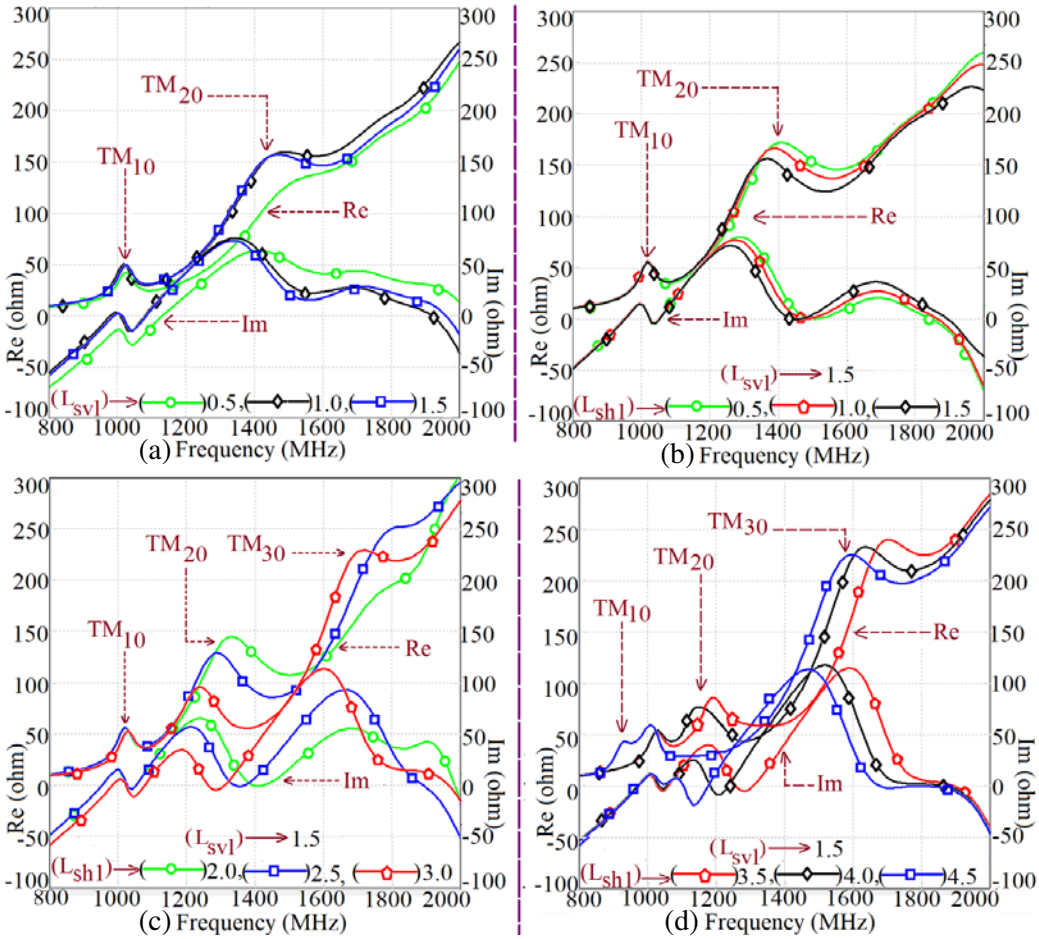

Figure 2. (a)–(d) Resonance curve plots for stub length 'L_{sh1}' and 'L_{sv1}' variations for the single stub loaded DP wideband Pi-shape MSA.

The simulated values of the respective modal frequencies are $f_{\mathrm{TM}_{10}} = 1008\,\mathrm{MHz}$, $f_{\mathrm{TM}_{20}} = 1555\,\mathrm{MHz}$, and $f_{\mathrm{TM}_{30}} = 1780\,\mathrm{MHz}$. As observed from the current distributions, the location of the current maxima amongst the subsequent modes is orthogonal. This will lead to the possible dual-polarized response. At TM_{10} mode, the Pi-shape MSA gives a BW of 215 MHz (18%). To realize further increase in the BW with possible dual polarization characteristics, tuning of the higher order modes, namely TM_{20} and TM_{30}, is required with respect to the fundamental TM_{10} mode. The preferable techniques for the tuning are either a slot embedded at minimum field positions or a stub placed near the maximum field locations, at the higher order modes. As per the present Pi-shape geometry, the stub technique is selected here. With reference to the surface current distribution shown in Fig. 1(d), the maximum field position of TM_{20} mode is present exactly in the middle of the top edge portion of the Pi-shape patch. Hence for the tuning of TM_{20} mode, an open circuit 'stub 1' with total length '$L_{sv1} + L_{sh1}$' and width 'W_s' is placed at the position 'X_1' as shown in Fig. 1(a).

For observing the effects and for optimizing the dimensions of the stub, a parametric study is carried out for the variation in 'L_{sv1}' and 'L_{sh1}', for 'W_s' = 0.8 cm. The corresponding resonance curve plots are as shown in Figs. 2(a)–(d). With an initial increment in the value of the 'L_{sv1}', TM_{20} and TM_{10} mode frequencies remain constant, as shown in Fig. 2(a). Hence, with retaining the compactness of the structure, horizontal stub length 'L_{sh1}' is increased further, while 'L_{sv1}' = 1.5 cm is kept constant. As the stub is placed near the minimum field location of TM_{10} mode, its frequency remains almost constant. With an increase in stub length 'L_{sh1}', TM_{20} mode frequency is reduced. This reduction is attributed to the placement of the stub exactly at the maximum field location of the TM_{20} mode. For 'L_{sh1}' = 3.0 cm and onwards, TM_{30} mode frequency is also reduced as shown in Figs. 2(c) and (d). This

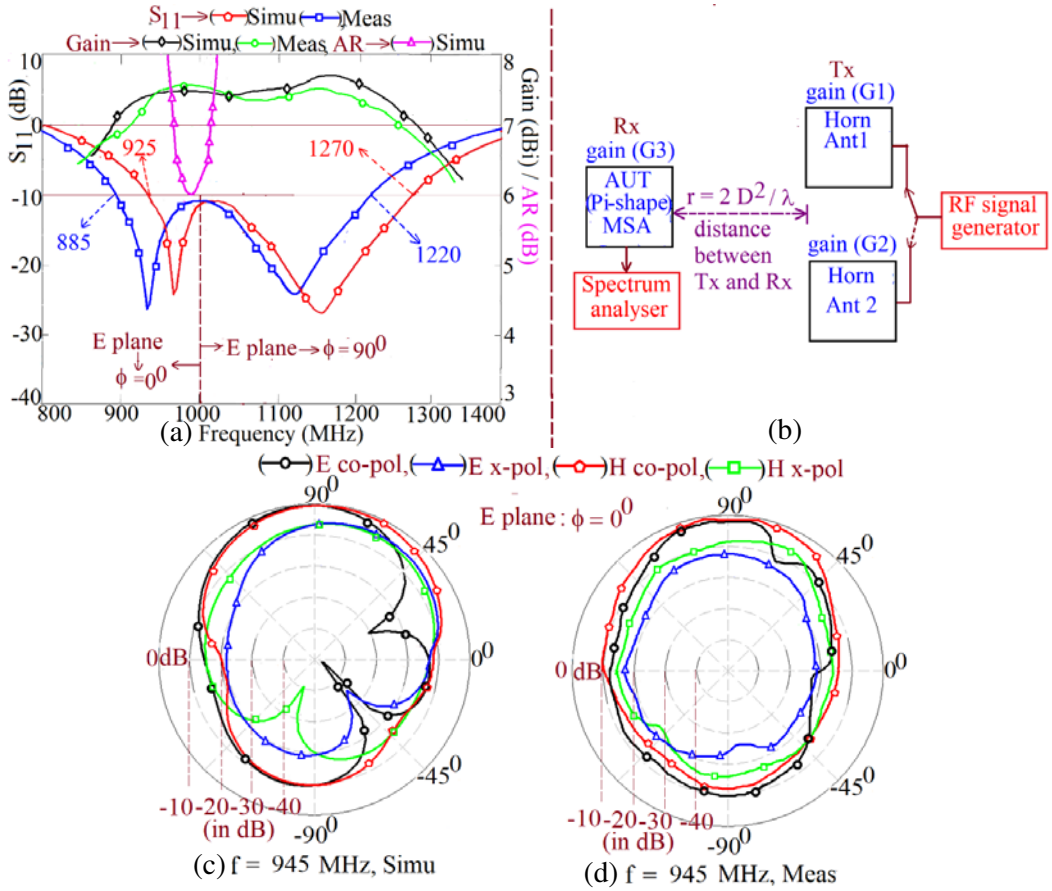

Figure 3. (a) S_{11}, gain, and AR plots, (b) block diagram for the three antenna gain method, and (c), (d) radiation pattern nearer to the band start frequency for the DP wideband single stub loaded Pi-shape MSA.

reduction is attributed to the placement of the stub near the maximum field position of the TM_{30} mode in the modified stub loaded Pi-shape patch. An optimum spacing between the TM_{20} and TM_{10} modes is obtained for 'L_{sh1}' = 3.5 cm, which realizes wider BW as shown in Fig. 2(d). Thus, the optimized wideband response is realized from a Pi-shape structure with a single open circuit L-shape bend stub. As the maximum of the surface currents is orthogonal across the TM_{10} and TM_{20} modes, single stub loaded Pi-shape MSA realizes wideband response showing dual polarization.

The optimized single stub loaded Pi-shape MSA is fabricated on a low-cost FR4 substrate and tested on a finite ground plane. The simulated and measured reflection coefficient (S_{11}) and gain plots along with the simulated axial ratio (AR) plot are as shown in Fig. 3(a). For the gain measurement, three antenna method is used, and the block diagram of the same is shown in Fig. 3(b). The simulated and measured radiation pattern plots observed near the band start and band-stop frequencies are shown in Figs. 3(b), (c) and 4(a), (b). The block diagram for the radiation pattern measurement is shown in Fig. 4(d). As per the given setup initially, the E-plane of the Pi-shape MSA (Antenna under test, AUT) is identified by rotating it in Φ-direction. Further, E co- and cross-polar measurements are carried out with respect to this orientation of AUT. The direction orthogonal to the E-plane is identified as the H-plane. Both the antennas are then aligned in their H-plane, and its co-polar and cross-polar measurements are carried out. The S_{11} values for the desired frequency BW are < -10 dB, giving simulated BW of 350 MHz (31%) whereas the measured BW is 335 MHz (30%). The antenna gain is above 7 dBi over the complete BW with a peak gain close to 8 dBi as shown in Fig. 3(a). Over the BW, for frequencies till 1001 MHz, E-plane is aligned along $\Phi = 0°$, while above 1001 MHz, E-plane is directed along $\Phi = 90°$. Thus, over 21% of BW, the proposed configuration offers horizontal polarization, and over 79% of the BW, design offers vertical polarization indicating the polarization agility. With appropriate selection of the proximity feed location also, the tuning in two polarizations

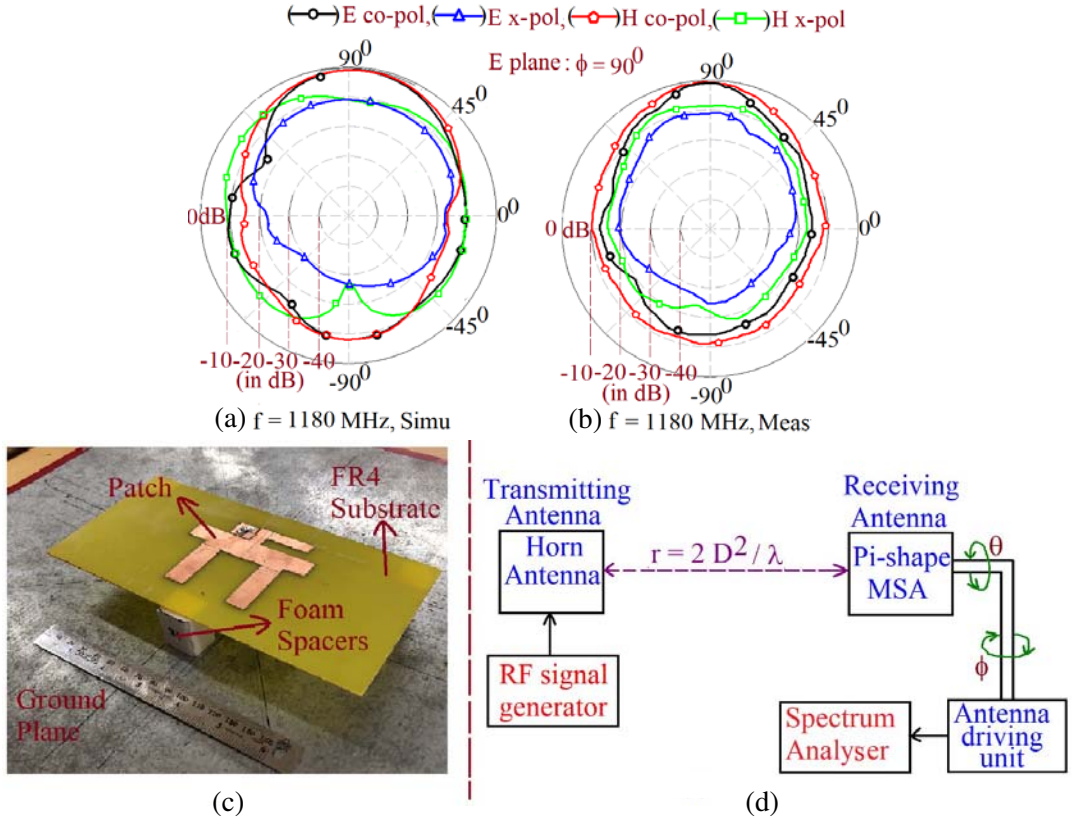

Figure 4. (a), (b) Radiation patterns nearer to the band stop frequency, (c) 3D side view of the fabricated antenna for the single stub loaded DP wideband Pi-shape MSA, and (d) block diagram of radiation pattern measurement set up.

BWs is possible as explained in [26]. Further, AR across the BW is more than 3 dB that indicates the dual-polarized response. The deviation in the measurement results from the simulation results is attributed to the variation in substrate parameters, feed point location, as well as marginal errors caused in the measurement setup. In wireless applications where the frequency and polarization agility are required in the same band of frequencies for avoiding the interference due to the frequency jamming or polarization jamming, dual-polarized wideband antennas can be used. As the proposed antenna yields wideband response with polarization agility, the proposed antenna satisfies the requirements of GSM-900 (890–915 MHz and 935-960 MHz) and navigation satellite communication bands (1164–1215 MHz). The fabricated antenna is shown in Fig. 4(c).

Further, for the realization of CP response in the optimized Pi-shape configuration, a close spacing between TM_{10} and TM_{20} resonant modes is needed with an equal contribution of the orthogonal surface current. These conditions are realized for 'L_{sh1}' = 4.5 cm that gives CP response, as shown in Fig. 2(d). For realizing this DP to CP polarization switching easily, a reconfigurable technique is used using the RF diode. For the biasing of the RF diode (BAR64-06W H6327) biasing circuits along with RFC (ELT-3KN131B) are used. The forward biased condition of the diode increases the stub length, whereas the reverse biasing of the diode reduces the length. Thus for the CP response, the stub length required is 'L_{sh1}' = 4.5 cm while for the DP response, 'L_{sh1}' = 3.5 cm is needed. The results for the CP

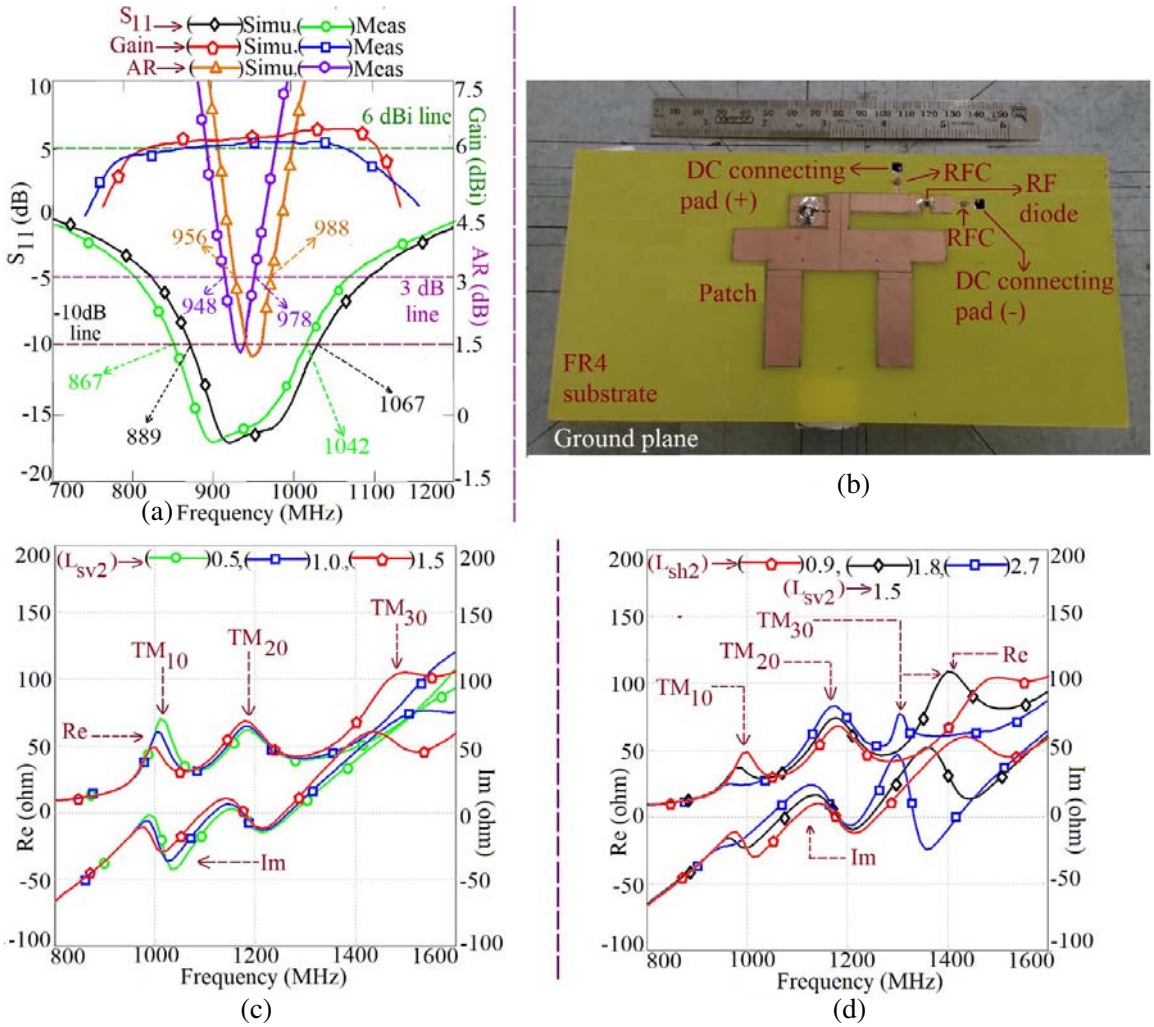

Figure 5. (a) S_{11}, gain and AR BW plots, and (b) top view of the fabricated reconfigurable antenna for the single stub loaded Pi-shape MSA, (c), (d) resonance curve plots for stub length 'L_{sh2}' and 'L_{sv2}' variations for the two stubs loaded DP wideband Pi-shape MSA design.

configuration showing S_{11}, gain, and AR BW plots are as given in Fig. 5(a). The simulated impedance BW is 178 MHz (17%), and AR BW (< 3 dB) is 32 MHz (3.0%). The corresponding measured values are 175 MHz (16%) and 27 MHz (2.7%). The smaller impedance BW is due to the reduction in the spacing in between the TM_{20} and TM_{10} resonant modes. The fabricated prototype for the reconfigurable design is shown in Fig. 5(b). Thus a single RF diode along with its integrated biasing circuit yields polarization switching within the stub loaded Pi-shape MSA design.

For further BW enhancement, tuning of TM_{30} mode is needed with respect to the lower order modes. Hence, without much disturbing TM_{10} and TM_{20} mode frequencies, the 'stub 2' dimensions are selected for the Pi-shape geometry. As per the surface current distribution, as shown in Fig. 1(e), the maximum of the field distribution at TM_{30} mode is along the extended length 'L_{extn}' of the basic Pi-shape patch. Hence, an open-circuit stub 'stub 2' with total length '$L_{sv2} + L_{sh2}$' and width 'W_s' is introduced at the position of 'X_2' as shown in Fig. 1(a). For observing the effects and for optimizing the configuration, a detailed parametric study for variations in 'L_{sv2}' and 'L_{sh2}', for 'W_s' = 0.8 cm is carried out. Those variations are highlighted in the resonance curves as shown in Figs. 5(c) and (d). For retaining the compactness, a similar bend L-shape stub is selected here. As the stub is placed exactly at the minimum field location of the TM_{20} mode, with the incrementing value of 'L_{sv2}', the TM_{20} mode frequency remains unchanged. As the stub is placed near the maximum current location of the TM_{10} mode, the decrement in its frequency is smaller while a larger reduction in the TM_{30} mode frequency is observed. An optimum spacing among the three resonant modes is obtained for 'L_{sv2}' = 1.5,

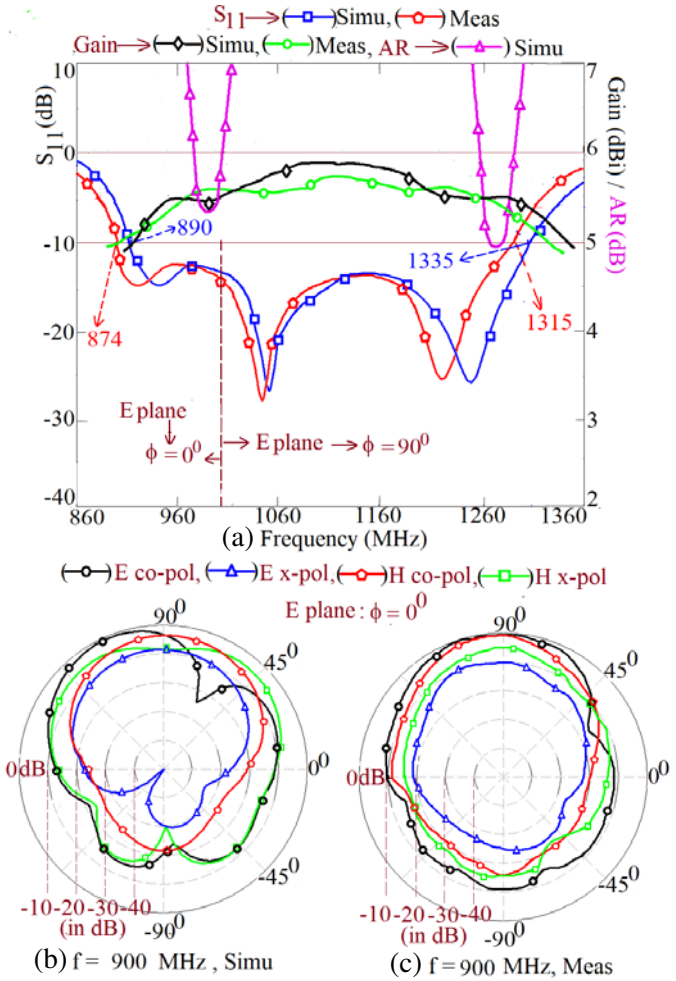

Figure 6. (a) S_{11}, gain and AR plots and (b), (c) radiation pattern near to the band start frequency for the DP wideband two stubs loaded Pi-shape MSA.

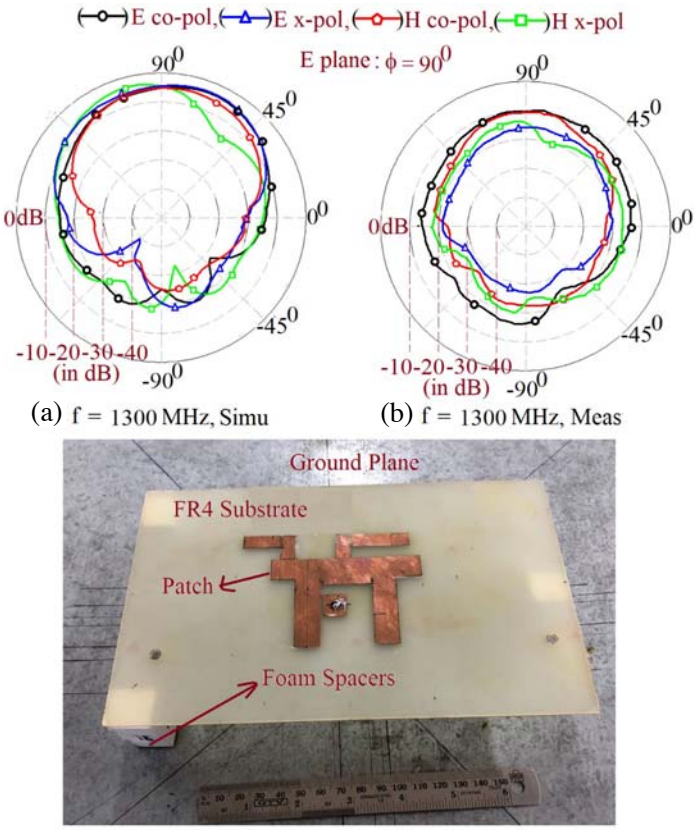

Figure 7. (a), (b) Radiation patterns nearer to the band stop frequency, and (c) 3D side view of the fabricated antenna for the DP wideband two stubs loaded Pi-shape MSA.

'L_{sh2}' = 2.7 cm, which yield wider BW as shown in Fig. 5(d). As the maximum of the surface currents is orthogonal across the three resonant modes, dual-stub loaded Pi-shape MSA also shows dual-polarized wideband response. An optimum response is obtained for 'L_{sub}' = 1.8, 'W_{sub}' = 0.8 cm. The measured and simulated S_{11}, gain plots, and simulated AR plot are as shown in Fig. 6(a). The simulated and measured radiation patterns observed at the two frequencies near the band start and band stop are shown in Figs. 6(b), (c) and 7(a), (b), respectively.

The simulated BW is 445 MHz (41%), while the measured BW is 441 MHz (40%). The antenna gain is greater than 5 dBi over the complete BW with a peak gain close to 6 dBi as shown in Fig. 6(a). The simulated AR value observed over the BW is more than 4 dB, which indicates the dual-polarized response. Over the VSWR BW, for frequencies till 1025 MHz, the E-plane is aligned along $\Phi = 0°$, while above 1005 MHz, the E-plane is directed along $\Phi = 90°$. Thus, over 25% of the BW, the proposed configuration offers horizontal polarization, and over 75% of the BW, vertical polarization is obtained, indicating the polarization agility. Thus, the proposed dual-polarized wideband antenna satisfies the requirements of the ISM 900 MHz band (902–928 MHz) with a center frequency of 915 MHz and navigation satellite communication bands (1164–1215 MHz and 1215–1240 MHz). The fabricated antenna is shown in Fig. 8(c). The proposed two stubs configuration of Pi-shape MSA occupies an area equivalent to the area of RMSA with length = 9.3 cm and width = 6.8 cm (area = 63.24 cm^2). For the air substrate thickness of 3.1 cm, this RMSA resonates at TM_{10} mode frequency of 1066 MHz and yields BW of 480 MHz (38%) with a single-polarization across it. In comparison, for the band start frequency of the BW, two stubs Pi-shape MSA yields nearly 11% reduction in the band start frequency and offers dual-polarized response over the BW, thereby offering the polarization agility.

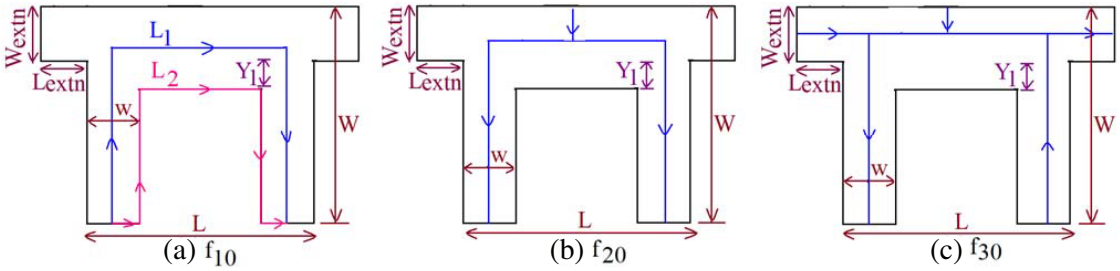

Figure 8. (a)–(c) Effective resonant lengths at different modes for basic Pi-shape MSA.

3. DESIGN METHODOLOGY FOR DUAL POLARIZED WIDEBAND PI-SHAPE MSA

The proposed designing methodology is based upon the parametric study and consequently the optimized configurations discussed in the previous section. Initially, the formulation in the resonant length is proposed for TM_{10}, TM_{20}, and TM_{30} modes. With respect to the current distributions shown in Figs. 1(c)–(d), the effective resonant length is marked for the basic Pi-shape MSA as shown in Figs. 8(a) and (c). At TM_{10} mode, since the surface currents flow around the inner patch edges and along the center-line in the Pi-shape patch, the average of lengths 'L_1' and 'L_2' is considered as given in Equations (1)–(3). The total length calculated for the TM_{10} mode is then equated to half the wavelength. The resonant length equation for TM_{20} mode as given in Equation (4) is equated to the wavelength variation. The extension length 'L_{extn}' and width 'W_{extn}' affect TM_{30} mode frequency only. Hence, their effects are considered while the TM_{30} mode resonant length is formulated, which is reflected in Equation (5). In Equations (3)–(5), 'ΔL' indicates the fringing field length which is a ratio of total substrate thickness $(h_a + h)$ and the square root of the effective dielectric constant (ε_{re}). Further, at TM_{30} mode, the resonant length is equated to three times of half the wavelength. As the proposed design uses air suspended dielectric, the value of effective dielectric constant 'ε_{re}' is calculated by using Equation (6). At the fundamental mode, the value of 'λ_g' is calculated by using Equation (7). These values are then used for calculating the frequency for the respective modes as given in Equation (8). In Equation (8), 'm' is an integer and takes a value as 1, 2, and 3 for the three modes. For the basic Pi-shape MSA at TM_{10} mode, the calculated frequency is found to be 995 MHz as against the simulated frequency of 1008 MHz, thereby giving '%Error' = 1.90%. For the TM_{20} mode, the simulated and calculated frequencies are 1555 and 1553 MHz, showing '%Error' = 1.29%. Lastly, at TM_{30} mode, simulated and calculated frequencies are 1780 and 1810 MHz that shows '% Error' of 1.6%, indicating the closer prediction between the calculated and simulated values. For the tuning of higher order mode frequency with respect to the fundamental patch mode, 'stub 1' and 'stub 2' are added in the basic Pi-shape MSA that yield dual-polarized wideband response. As per the parametric study carried out concerning the stub length variations, it is clear that 'stub 1' affects both TM_{20} and TM_{30} mode frequencies while 'stub 2' mainly affects the TM_{30} mode frequency. Hence, further formulations at these resonant modes are obtained by adding the total stub length ('$L_{sv1}+L_{sh1}$' and '$L_{sv2}+L_{sh2}$') effect on the respective mode resonant lengths as given in Equations (10)–(11). The frequency calculated for this increment in the total stub length using Equation (8) agrees closely with the simulated result, as shown in Figs. 9(a)–(c). Using the proposed formulation at each mode of the Pi-shape geometry, a % Error of less than 5% is obtained. Further redesigning of stub loaded Pi-shape MSAs is presented for the fundamental mode frequencies of 800 and 1600 MHz.

$$L_1 = 2\left[W - \frac{w}{2}\right] + L - w \tag{1}$$

$$L_2 = 2\left[W - w\right] + (L - 2w) + w \tag{2}$$

$$L_{eff10} = \frac{L_1 + L_2}{2} + 2\left(0.35\Delta L\right) \tag{3}$$

$$L_{eff20} = \frac{L_1 + L_2}{2} + 2\left(\Delta L\right) \tag{4}$$

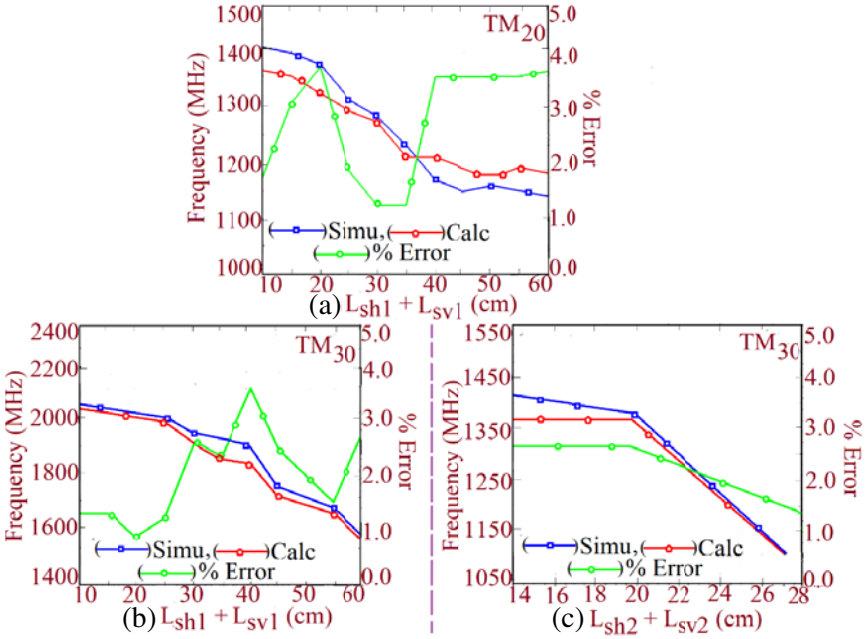

Figure 9. Frequency and % error plots at (a) TM_{20}, (b) TM_{30} modes using stub 1 and (c) TM_{30} mode using stub 2, for the stub loaded DP wideband Pi-shape MSA variations.

$$L_{eff30} = \frac{L_1 + L_2}{2} + 2(\Delta L) + 2(W_{extn} + L_{extn}) \tag{5}$$

$$\varepsilon_{re} = \varepsilon_r(h + h_a) \Big/ \varepsilon_r h_a + h \tag{6}$$

$$\lambda_g = 30 \Big/ f_{\mathrm{TM}_{10}} \sqrt{\varepsilon_{re}} \tag{7}$$

$$f_{m,0} = (30m) \Big/ (2L_{effm\cdot 0}\sqrt{\varepsilon_{re}}) \tag{8}$$

$$\%\,\mathrm{Error} = \left| \frac{f_{\mathrm{simu}} - f_{\mathrm{calc}}}{f_{\mathrm{simu}}} \right| \tag{9}$$

$$L_{eff20stub} = L_{eff20} + L_{sv1} + L_{sh1} \tag{10}$$

$$L_{eff30stub} = L_{eff30} + L_{sv1} + L_{sh1} + L_{sv2} + L_{sh2} \tag{11}$$

As the proposed design uses an air suspended substrate, the value of effective dielectric constant 'ε_{re}' needs to be calculated first. Since the value of air gap 'h_a' is unknown, in the initial calculation, the value of 'ε_{re}' is assumed to be 1.06. For the given fundamental TM_{10} mode frequency, the value of 'λ_g' is calculated by using Equation (7). Based upon the optimized design discussed above, the total substrate thickness 'h_t' = $(h_a + h)$ in the redesigned configuration is selected as $0.1\lambda_g$. Further, the practically realizable value of 'h_a' is selected, and using this value, 'ε_{re}' and 'λ_g' are recalculated by using Equations (6) and (7), respectively. By using the new value of 'ε_{re}', 'h_t' and 'h_a' are recalculated. In this iterative procedure, it was observed that the value of practically realizable 'h_a' marginally changes concerning the earlier value calculated.

Hence, the initial calculated value of 'h_a' is maintained. This iterative procedure is needed here since the value of 'ε_{re}' is initially unknown. Further, a new value of 'ε_{re}' is then used for calculating the frequency of the respective modes, as given in Equation (8). For deciding the dimensions of the redesigned basic Pi-shape configuration, the physical length 'L_p' is calculated by using Equation (12) for the TM_{10} mode. With reference to the resonant length path as shown in Fig. 8(a), length 'L_p' is expressed in terms of the basic Pi-shape patch dimensions 'L' and 'W' as given in Equation (13). A

similar ratio between various Pi-shape patch parameters as present in the above optimum design is considered. Hence, outer edge dimensions are selected to be the same, i.e., 'L' = 'W', and Pi-shape width is selected as 'w' = 0.245 W. Thus, by substituting these values in Equation (13), the Pi-shape patch outer edge length is expressed as $L = 0.418L_p$. Based upon the optimized configuration above, other patch parameters are expressed in terms of 'L_p'; as inner edge length 'l_{in}' = $0.2132L_p$, inner edge width 'w_{in}' = $0.3156L_p$, extension length and width as '$W_{extn} = L_{extn}$' = $0.102L_p$. Apart from the stub length, their positions, 'X_1', 'X_2', and stub width, 'W_s', also affect the respective mode frequencies. However, the trend in the variations of modal frequencies is largely governed by stub lengths. As per the optimized configuration, 'stub 1' is placed exactly at the center of the outer patch edge, i.e., at 'X_1' = $L/2$, while 'stub 2' is placed along the extended patch length, i.e., at 'X_2' = $0.307L_{extn}$. Similarly, the stub width 'W_s' is expressed in terms of the main patch length, as 'W_s' = $0.150L$.

$$L_p = C/\left(2f_{10}\right)\left(\sqrt{\varepsilon_{re}}\right) - 2(0.35\Delta L) \tag{12}$$

$$L_p = 2\left[W - \frac{w}{2}\right] + L - w + 2\left[W - w\right] + (L - 2w) + w \Big/ 2 \tag{13}$$

As per the parametric study, 'stub 1' length variation affects both TM_{20} and TM_{30} modes. For the given stub length, optimum dual-polarized wideband response in the single stub configuration is obtained for the frequency ratio 'TM_{20}/TM_{10}' of 1.21 and aspect ratio '$W_s/L_{sv1} + L_{sh1}$' of 6.3, while the CP response is realized for the frequency ratio of 1.05. Using Equations (1)–(12), the f_{10}, f_{20}, and f_{30} mode frequencies against the stub length variations are obtained, and the ratio plots for them are shown in Figs. 10(a) and (b). The value of 'stub 1' length that gives the desired frequency and aspect ratio is noted. Similarly, as per the parametric study, 'stub 2' length variation affects the TM_{30} mode. For the optimum two stubs Pi-shape configuration, an optimum dual-polarized wideband response is obtained for the dual-frequency ratio 'TM_{30}/TM_{10}' of 1.33 and 'TM_{30}/TM_{20}' of 1.17 with an aspect ratio '$W_s/L_{sv2} + L_{sh2}$' = 5.2. Using the formulations given in Equations (1)–(12), the f_{10}, f_{20}, and f_{30} mode frequencies against stub length variations are obtained, and the ratio plots for them are as shown in Figs. 10(c) and (d). The value of stub length that realizes the desired frequency and aspect ratio are noted. For antenna excitation, a square proximity strip of length 'L_s' = $0.4\lambda_g$ is placed at the same thickness as that of the Pi-shape patch. The position of this strip for the single stub configuration is at 'x_f, y_f' = $0.048\lambda_g$, $0.175\lambda_g$, while for the two stubs configuration, it is at 'x_f, y_f' = $0.068\lambda_g$, $0.079\lambda_g$. These values are selected from the optimized configurations discussed above. Using these guidelines,

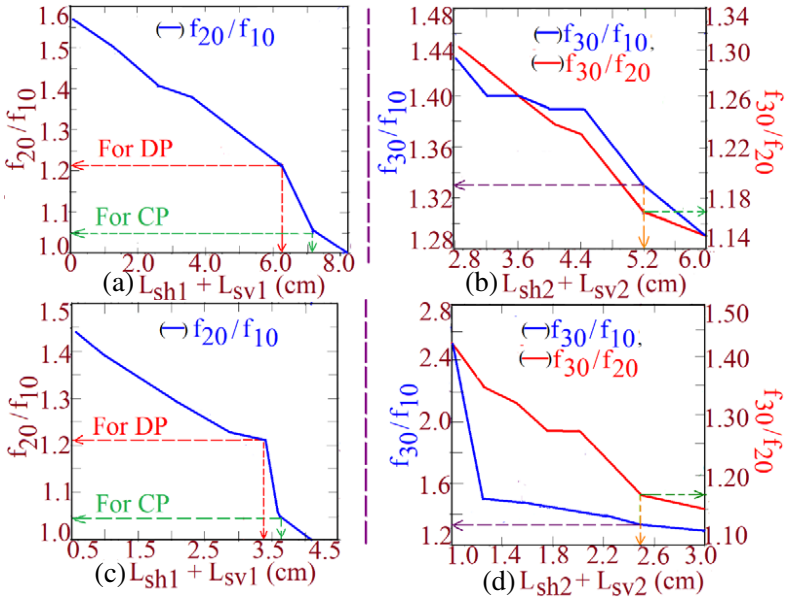

Figure 10. Frequency ratio plots among TM_{10}, TM_{20}, and TM_{30} modes for single stub and two stubs Pi-shape MSA for (a), (b) 800 MHz, and (c), (d) 1600 MHz.

Table 1. Various antenna parameters for the re-designed DP wideband Pi-shape MSAs.

Antenna Parameters	$f_{TM1,0} = 800$ MHz				$f_{TM1,0} = 1600$ MHz			
(L, W)	(6.6, 6.6) cm				(3.3, 3.3) cm			
w, Y_1	1.6, 0.5 cm				0.8, 0.3 cm			
(L_{in}, W_{in})	(3.4, 5.0) cm				(1.7, 2.5) cm			
(L_{extn}, W_{extn})	(1.6, 1.6) cm				(0.8, 0.8) cm			
(X_1, X_2)	(3.3, 0.5) cm				(1.6, 0.3) cm			
(x_{f1}, y_{f1}), (x_{f2}, y_{f2}),	(1.8, 7.4) cm, (2.5, 2.9) cm				(0.9, 3.8) cm, (1.2, 1.4) cm			
l_s	1.5 cm				0.8 cm			
W_s	1.0 cm				0.5 cm			
(L_{sh1}, L_{sv1})	(4.4, 1.9) cm				(2.2, 0.9) cm			
(L_{sh2}, L_{sv2})	(3.2, 0.2) cm				(1.6, 0.9) cm			
	Single stub Config.		**Two stubs Config.**		**Single stub Config.**		**Two stubs Config.**	
	Simu	**Meas**	**Simul**	**Meas**	**Simu**	**Meas**	**Simul**	**Meas**
Bandwidth MHz (%)	330 (31)	315 (29)	370 (35)	368 (33)	729 (39)	710 (38)	834 (41)	830 (40)
Gain (dBi)	6	5.5	5.5	5	6	5	5.5	5

single and two stubs Pi-shape MSAs are designed for the fundamental mode frequencies of 800 MHz and 1600 MHz. The redesigned antennas are simulated, and experimentation is done. Various antenna parameters for the redesigned configurations are given in Table 1.

The simulated and measured S_{11}, gain and simulated AR plots for the two stub configuration are provided in Figs. 11(a) and (b). In all the redesigned configurations, similar results to that observed in the proposed configuration are obtained. As noted from the S_{11} plots, the band start frequency in the two redesigned configurations is around the desired fundamental mode frequency. Thus, the given procedure can be used to redesign similar dual polarized wideband Pi-shape MSAs around the given fundamental mode frequency. Fabricated prototype for the antenna redesigned at 1600 MHz is as shown in Figs. 11(c) and (d). A detailed comparison for the proposed wideband Pi-shape MSAs against the reported configurations is presented below in Table 2.

The MSA reported in [13] employs the combination of a metallic cone and two feeding networks. Against that the proposed configuration employs a single feed and stubs for the realization of DP wideband response. Multiple patch parameters and complex feeding techniques are used in the designs reported in [14–17]. Although wider BW using compact design is reported in [18], it lacks in providing an in-depth explanation about the patch modes concerning the overlapping patches. Though the antenna is fabricated on thicker multiple substrates, its BW realized in [19] is smaller. A combination of bowtie patches with T-shape slots is used in [20], while embedded rectangular slots are used for polarization tuning in [21]. Also, a magnetically coupled loop with hook shape probes along with shorting pins is used for the realization of DP response in [22]. However, these configurations lack in providing detailed explanations about the patch modes concerning the shorting pins or vias and embedded slots, which is required for an in-depth understanding of the antenna functioning. Against these, for the proposed configurations in this paper, an in-depth parametric analysis, explaining the effect of the stub dimensions on polarization tuning and wider BW concerning the antenna modes, is provided. For the tuning of the polarization and BW, varactor or PIN, diodes are used in [23, 24]. Against them, the proposed DP configuration yields polarization and BW tuning by changing the individual stub dimensions for the individual patch modes. Configurations presented in [27–30] offer nearly the same BW as compared with the proposed design. However, they provide a single polarized response with

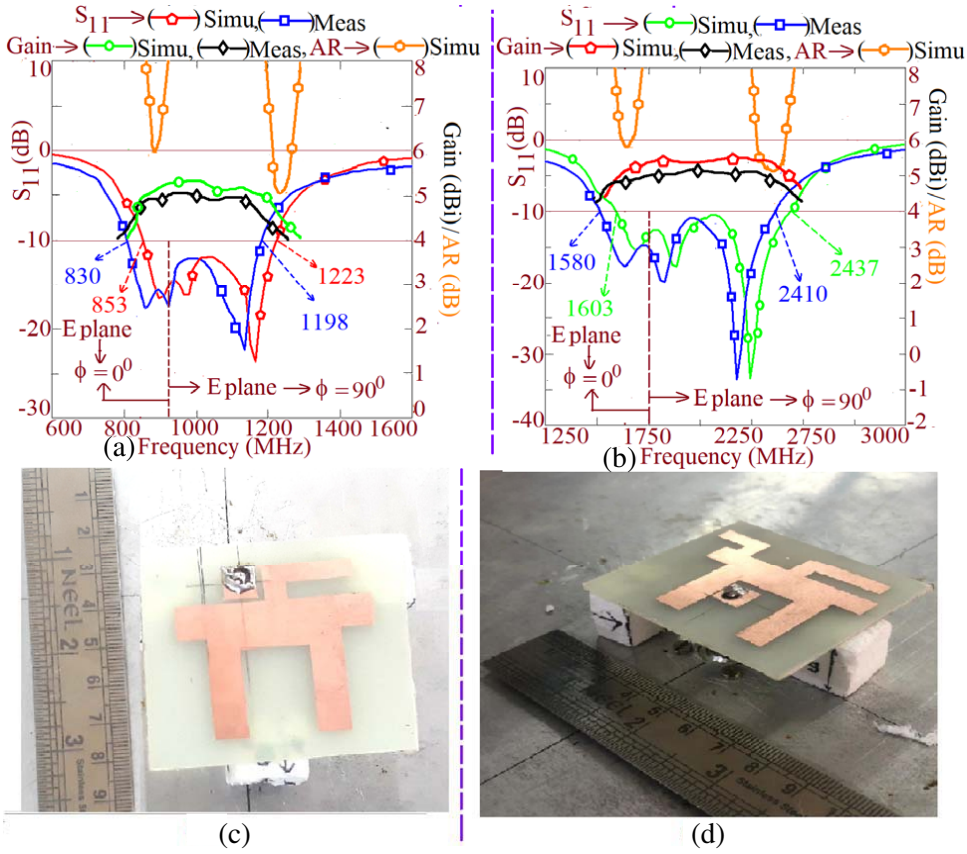

Figure 11. S_{11}, gain, and AR plots for the redesigned two stubs Pi-shape MSA at (a) 800 MHz, (b) 1600 MHz and fabricated antenna for (c) single stub, (d) two stubs configuration at 1600 MHz.

a larger patch size. Wideband and compact designs are reported in [31, 32]. However, the reported design does not provide any polarization agility. Also, the reported works lack in providing any design methodology. Against it, the proposed configuration is compact and yields dual-polarized response. Also, the design methodology for redesigning similar types of antennas for different fundamental mode frequencies is provided in the present study. A characteristics mode analysis for the planar wideband configuration is reported in [33]. However, it is not useful in the redesigning of similar configurations at different frequencies. In comparison, an in-depth design methodology based on the resonant length formulation is provided in the present work.

Thus, in contrast with the reported papers, this paper presents a simple proximity fed Pi-shape MSA for the dual-polarized wideband response offering BW $> 35\%$ and gain > 6 dBi. To the best of the authors' knowledge, a few reported papers do discuss the dual-polarized wideband MSA designs using the stubs or slots. However, an in-depth study to put forward an explanation about DP wideband response in terms of the resonant patch modes and subsequent design methodology based on the formulation is missing. The proposed work clearly explains the impedance matching of higher order modes together with the fundamental mode using the variations in stub dimensions for the tuning of dual polarizations and wider BW. The configurations fabricated on an air suspended low cost FR4 substrate yield significant BW and gain across the spectrum. Compared with the conventional rectangular MSA, which has equivalent outer patch dimensions as that of Pi-shape geometry, the proposed configuration offers 11% reduction in the band start frequency. Thus, the proposed antenna configuration is simpler and compact in construction with better impedance BW and gain, thus satisfying the requirements of polarization agility. Also, it covers wireless applications like GSM900/navigation satellite/ISM 900. These are all new technical contributions in the proposed work against the reported DP wideband MSAs.

Table 2. Comparison between DP wideband Pi-shape MSA against reported DP wideband MSAs.

MSA shown in	BW (MHz, %)	Tuning element	Peak Gain (dBi)	Area, thickness (A/λ_c, h/λ_c)
Fig. 4(c)	**335, 30**	**Single stub**	**7.5**	$\mathbf{1.8\lambda_c, 0.11\lambda_c}$
Fig. 7(c)	**441, 40**	**Two stubs**	**5.5**	$\mathbf{2.3\lambda_c, 0.12\lambda_c}$
Ref. [12]	1000, 45	—	—	$1.70\lambda_c$, $0.235\lambda_c$
Ref. [13]	1560, 29	metallic cone	9.5	$1.86\lambda_c$, $0.07\lambda_c$
Ref. [14]	1400, 39	—	10	$1.2\lambda_c$, $0.016\lambda_c$
Ref. [15] ant 3	At port 1: 1040, 27 At port 2: 640, 19	slots	8.5	2. $1\lambda_c$, $0.08\lambda_c$
Ref. [17]	1260, 56.3	slots	6	$1.62\lambda_c$, $0.035\lambda_c$
Ref. [18]	3000, 50	Square patches	6	$4.67\lambda_c$, $0.06\lambda_c$
Ref. [19]	At V port: 700, 25 At H port: 690, 24	—	—	$1.29\lambda_c$, $0.114\lambda_c$
Ref. [20]	At port 1: 1030, 46 At port 2: 1120, 56	slots	9	$1.25\lambda_c$, $0.1\lambda_c$
Ref. [21]	1090, 49	slots	8.7	$4.1\lambda_c$, $0.27\lambda_c$
Ref. [22]	At Port 1: 1250, 40 At port 2: 1250, 38	—	9	$1.64\lambda_c$, $0.062\lambda_c$
Ref. [23]	410, 29	Varactor diodes	—	$1.03\lambda_c$, $0.014\lambda_c$
Ref. [27]	380, 14	—	7	$5.17\lambda_c$, $0.04\lambda_c$
Ref. [28]	260, 13	—	7	$5.6\lambda_c$, $0.0292\lambda_c$
Ref. [29]	340, 6	—	11	$4.9\lambda_c$, $0.014\lambda_c$
Ref. [30]	2020, 68	—	6, 9.6	$1.55\lambda_c$, $0.02\lambda_c$
Ref. [31]	330, 6.8	—	7	$0.5\lambda_c$, $0.027\lambda_c$
Ref. [32]	410, 8.4	—	8	$0.79\lambda_c$, $0.026\lambda_c$
Ref. [33]	2200, 81	—	1.5, 2.5	$1.57\lambda_c$, $0.014\lambda_c$

4. CONCLUSIONS

A compact design of a stub-loaded Pi-shape MSA for dual-polarized wideband response is presented. The proposed work provides a detailed explanation for the antenna working in terms of the patch resonant modes. The stubs in the Pi-shape patch tune the TM_{20} and TM_{30} mode frequencies with respect to TM_{10} mode, to yield more than 430 MHz ($> 35\%$) of BW. The stub length changes the spacing among three modal frequencies, and proximity feed position decides the coupling to the two modes, which can yield variable polarization BW. The proposed compact designs with single and dual stub configurations show broadside radiation patterns across the BW with a broadside gain above 5 dBi. The proposed single patch design can entirely cover wireless applications like GSM900/navigation satellite/ISM900 yielding polarization agility. Redesigned guidelines are proposed based on the parametric analysis done. Antennas designed using the proposed guidelines yield similar dual-polarized wideband response showing impedance BW $> 35\%$.

REFERENCES

1. Garg, R., P. Bhartia, and I. Bahl, *Microstrip Antenna Design Handbook*, Artech House, London, 2001.

2. Kumar, G. and K. P. Ray, *Broadband Microstrip Antennas*, 1st Edition, Artech House, USA, 2003.
3. Wong, K. L., *Compact and Broadband Microstrip Antennas*, 1st Edition, John Wiley & Sons, Inc., New York, USA, 2002.
4. Balanis, C. A., *Antenna Theory & Design*, 3rd Edition, John Wiley & Sons, Inc., 2005.
5. Zhao, F., W. Zhang, L. G. Han, and R. Yang, "A wideband dual-polarized patch antenna fed with the aperture-coupled microstrip," *Electromagnetics*, Vol. 38, No. 1, 58–69, 2018.
6. Ghorbani, K. and R. B. Waterhouse, "Dual polarized wide-band aperture stacked patch antennas," *IEEE Transactions on Antennas and Propagation*, Vol. 52, No. 8, 2171–2175, 2004.
7. Row, J.-S., S. H. Yeh, and K. L. Wong, "Compact dual-polarized microstrip antennas," *Microwave and Optical Technology Letters*, Vol. 27, No. 4, 284–287, 2004.
8. Lam, K. Y., K. M. Luk, K. F. Lee, H. Wong, and K. B. Ng, "Small circularly polarized U-slot wideband patch antenna," *IEEE Antennas and Wireless Propagation Letters*, Vol. 10, 87–90, 2011.
9. Wong, K.-L., C. T. Hao, and W. C. Tzung, "Broadband dual-polarized aperture-coupled patch antennas with modified H-shaped coupling slots," *IEEE Transactions on Antennas and Propagation*, Vol. 50, No. 2, 188–191, 2002.
10. Wong, K.-L. and T. W. Chiou, "Broadband dual-polarized patch antennas fed by capacitively coupled feed and slot-coupled feed," *IEEE Transactions on Antennas and Propagation*, Vol. 50, No. 3, 346–351, 2002.
11. Deshmukh, A. A., S. Pawar, A. G. Ambekar, P. Kamble, and K. P. Ray, "Compact Y-shape antenna for dual polarized wideband response," *IEEE Applied Electromagnetics Conference (AEMC)*, 1–2, Aurangabad, 2017.
12. Jin, Y. and Z. Du, "Broadband dual-polarized F-probe fed stacked patch antenna for base stations," *IEEE Antennas and Wireless Propagation Letters*, Vol. 14, 1121–1124, 2015.
13. Shad, S., Z. Rahimian, and M. Bemani, "Design of a wideband dual-polarized microstrip patch antenna with novel structure for WLAN application," *Microwave and Optical Technology Letters*, Vol. 58, No. 7, 1599–1602, 2016.
14. Ryu, K. S. and A. A. Kishk, "Wideband dual-polarized microstrip patch excited by hook shaped probes," *IEEE Transactions on Antennas and Propagation*, Vol. 56, No. 12, 3645–3649, 2008.
15. Xie, J.-J., Y.-Z. Yin, J. Ren, and T. Wang, "A wideband dual-polarized patch antenna with electric probe and magnetic loop feeds," *Progress In Electromagnetics Research*, Vol. 132, 499–515, 2012.
16. Xue, M., J. Liu, Z. Zhao, X. Yang, and Y. Ying, "Wideband dual polarized hybrid fed patch antenna," *International Journal of RF Microwave Computer Aided Engineering*, Vol. 29, No. 6, 2019.
17. Lian, R., S.-F. Zheng, Y.-Z. Yin, J. Wu, S. Zhang, and G. Zhang, "A single-layer wideband dual-polarized antenna with high isolation," *Progress In Electromagnetics Research C*, Vol. 49, 115–122, 2014.
18. Rambabu, K., M. Alam, J. Bornemann, and M. A. Stuchly, "Compact wideband dual-polarized microstrip patch antenna," *IEEE Antennas and Propagation Society Symposium*, Vol. 2, 1955–1958, CA, USA, 2004.
19. Gao, S. C., L. W. Li, M. S. Leong, and T. S. Yeo, "A novel dual-polarized, wide-band microstrip patch antenna with aperture coupling," *IEEE Antennas and Propagation Society International Symposium, Digest*, Vol. 4, 78–81, Held in Conjunction with: USNC/URSI National Radio Science Meeting, Boston, MA, USA, 2001.
20. Li, B., Y.-Z. Yin, H. Wei, D. Yang, and Y. Zhao, "Wideband dual-polarized patch antenna with low cross polarization and high isolation," *IEEE Antennas and Wireless Propagation Letters*, Vol. 11, 427–430, 2012.
21. Tang, Z., J. Liu, Y. M. Cai, J. Wang, and Y. Yin, "A wideband differentially fed dual-polarized stacked patch antenna with tuned slot excitations," *IEEE Transactions on Antennas and Propagation*, Vol. 66, No. 4, 2055–2060, 2018.

22. Xie, J. J., X. L. Liu, Y. Z., and J. H. Wang, "Wideband dual-polarized electromagnetic-fed patch antenna with high isolation and low cross-polarization," *Electronics Letters*, Vol. 49, No. 3, 171–173, 2013.
23. Babakhani, B. and S. Sharma, "Wideband frequency tunable concentric circular microstrip patch antenna with simultaneous polarization reconfiguration," *IEEE Antennas and Propagation Magazine*, Vol. 57, No. 2, 203–216, 2015.
24. Yang, Z.-X., H.-C. Yang, J.-S. Hong, and Y. Li, "Bandwidth enhancement of a polarization-reconfigurable patch antenna with stair-slots on the ground," *IEEE Antennas and Wireless Propagation Letters*, Vol. 13, 579–582, 2014.
25. CST Microwave Studio, Version 2019.
26. Ambekar, A. G., A. A. Deshmukh, S. Pawar, and K. P. Ray, "Dual polarized variations of p-shape microstrip antenna loaded with stub," *Proceedings of International Conference on Wireless Communication. Lecture Notes on Data Engineering and Communications Technologies Springer*, Vol. 36, 257–266, 2020.
27. Liu, N.-W., L. Zhu, W. W. Choi, and G. Fu, "A low-profile wideband aperture-fed microstrip antenna with improved radiation patterns," *IEEE Transactions on Antennas and Propagation*, Vol. 67, No. 1, 2018.
28. Liu, N., L. Zhu, and W. Choi, "A differential-fed microstrip patch antenna with bandwidth enhancement under operation of TM10 and TM30 modes," *IEEE Transactions on Antennas and Propagation*, Vol. 65, No. 4, 1607–1614, 2017.
29. Wen, J., D. Xie, and L. Zhu, "Bandwidth-enhanced high-gain microstrip patch antenna under TM30 and TM50 dual-mode resonances," *IEEE Antennas and Wireless Propagation Letters*, Vol. 18, No. 10, 1976–1980, 2019
30. Radavaram, S. and M. Pour, "Wideband radiation reconfigurable microstrip patch antenna loaded with two inverted U-slots," *IEEE Transactions on Antennas and Propagation*, Vol. 67, No. 3, 1501–1508, 2019.
31. Yoo, J. U. and H.-W. Son, "A simple compact wideband microstrip antenna consisting of three staggered patches," *IEEE Antennas and Wireless Propagation Letters*, Vol. 19, No. 12, 2038–2042, 2020.
32. Zhang, J., L. Zhu, Q. Wu, N. Liu, and W. Wu, "A compact microstrip-fed patch antenna with enhanced bandwidth and harmonic suppression," *IEEE Transactions on Antennas and Propagation*, Vol. 64, No. 12, 5030–5037, 2016.
33. Perli, B. R. and A. M. Rao, "Characteristic mode analysis of wideband microstrip antenna," *Progress In Electromagnetic Research C*, Vol. 97, 201–212, 2019.